Theory of low-energy electron diffraction for detailed structural determination of nanomaterials – ordered structures

G. M. Gavaza[(1)], Z. X. Yu[(1,2)], L. Tsang[(4)], C. H. Chan[(3)], S. Y. Tong[(1)], M. A. Van Hove[(1)]
[(1)] Department of Physics and Materials Science, City University of Hong Kong, Hong Kong
[(2)] Department of Physics, Zhongshan University, Guangzhou, China
[(3)] Department of Electronic Engineering, City University of Hong Kong, Hong Kong
[(4)] Department of Electrical Engineering, University of Washington, Seattle, Washington, USA

Receipt Date: _____

Abstract

To enable the determination of detailed structures of nanomaterials, we extend the theory of low-energy electron diffraction (LEED) to become more efficient for complex and disordered systems. Our new cluster approach speeds up the computation to scale as $n \log n$, rather than the current n^3 or n^2, with n the number of atoms, for example, making nanostructures accessible. Experimental methods to measure LEED data already exist or have been proposed. Potential application to ordered nanoparticles are illustrated here for C_{60} molecules adsorbed on a Cu(111) surface, with and without co-adsorbed metal atoms, as well as for adsorbed carbon nanotubes. These demonstrate sensitivity to important structural features such as size and deformation of the nanostructures.

PACS: 61.14.Dc, 61.14.Hg, 61.46.-w, 61.48.+c

1. Introduction

Nanomaterials open up new fields of science and hold great promise for many novel applications [1,2]. As in other fields (such as solid-state physics, chemistry and biology), the atomic-scale structure plays a fundamental role, especially in understanding and predicting a multitude of useful materials properties: this includes in particular bond lengths and bond angles.

Such information is now sorely missing, for lack of suitable techniques to obtain it from experiment. Few techniques are currently available, and none has yet been used to our knowledge, to determine the detailed atomic-scale structure of nanomaterials from experiment with the precision needed to calculate their properties, i.e. on the scale of 0.01 nm = 0.1 Å or better. X-ray diffraction (XRD), due to relatively weak light sources, is a candidate for complex structures that are periodic and well-prepared[3]. X-ray absorption fine structure (XAFS) is much more tolerant of long-range disorder, but less capable of

handling the mix of inequivalent atomic environments typical of nanostructures[4]. Scanning tunneling microscopy (STM) can provide impressive atomic-scale images of single nanostructures, but requires theoretical modeling to extract bond lengths and angles, and in some cases even the presence or absence of atoms[5]. Theory, whether phenomenological or using first principles, can predict nanostructural details, but must itself be checked against determination from experiment; this is especially true for complex structures that require approximations in the theory and that allow many alternative structures of nearly the same total energy.

We prove conclusively in this work that low-energy electron diffraction (LEED) offers great promise for the detailed structural determination of many nanomaterials: our work exhibits the possibility to perform the needed calculations, despite the large complexity of typical nanostructures. In this paper, we develop the main elements of the methodology and illustrate the potential of our method for periodically ordered nanostructures (as briefly reported earlier[6]), while the application to isolated or disordered nanostructures will be described separately[7].

An important question remains: can LEED experiments be successfully conducted on nanomaterials? LEED experiments have already produced diffraction patterns from arrays of ordered nanoparticles, such as adsorbed buckminsterfullerenes[8]; it would thus be a routine matter to measure their diffracted intensities with existing equipment.

For less well-ordered nanostructures, it should be possible to focus the incident LEED beam onto a single particle or small area and record the diffracted pattern, either as angular dependent intensity data or as energy-dependent data ("I-V curves"): this has been proposed in the form of convergent-beam LEED (CBLEED)[9]; diffraction from single objects as small as a few nanometers is then conceivable. The angular spread of the converging beam then implies a corresponding broadening of the diffraction pattern. Even for a diffuse LEED pattern (without sharp spots due to absence of long-range periodicity) this would still be valuable if this spread is taken into account in the calculation through convolution (as is already commonly done in photoelectron diffraction[10], for example). In the case of an ordered structure, the sharp spots of normal LEED would be replaced by disks delimited by the angular spread of the convergent beam: these disks contain angle-dependent intensities that provide additional structural information not present in sharp spots.

Another approach is to use an STM tip as electron source to form a very narrow beam[11]: such an experiment has already produced diffraction patterns from areas as small as 400 μm across, with areas smaller than 50 nm across being possible; electron beams have in fact been focused to such dimensions in various applications[12].

LEED requires a theory to extract structural information, mainly due to strong multiple scattering of the diffracted electrons: electrons often scatter from several atoms in succession before leaving the material for the detector[13,14]. The multiple scattering, which can be formulated as the solution of a matrix-vector equation $Ax = b$, requires compute times that scale as N^3 for matrix inversion or N^2 for some iterative schemes, as

implemented in existing LEED codes; here the matrix dimension N is proportional to the number of inequivalent atoms n and the number of partial spherical waves used (typically ~100). Such power-law scaling can be very challenging for nanostructures, for which n can be in the hundreds and N in the many thousands or more.

The present work develops a theoretical scheme that scales much more favorably, namely as $N \log N$ and thus $n \log n$, making nanostructures accessible. It uses a cluster approach based on mathematical methods developed in the context of the multiple scattering of electromagnetic waves[15,16]. Our adaptation of these methods is shown here to permit the calculation of LEED intensities for nanostructures. We have chosen to test our methods on several representative nanosystems. We have thus modeled buckminsterfulleres (C_{60}) and carbon nanotubes (CNT) adsorbed on a Cu(111) surfaces; these are ordered with relatively large supercells on the Cu(111) substrate. We will report on similar modeling for isolated or disordered nanostructures separately[7].

Since the aim is to enable structural determination, we investigated the structural sensitivity of LEED by varying representative geometrical parameters of the various nanostructures.

2. Method

Nanostructures are a serious challenge for LEED calculations. The main reason is that one of the theory's components, the solution of a $Ax = b$ matrix-vector equation becomes a computational bottleneck. The standard LEED codes solve this equation by inverting the matrix A by any of various schemes; this approach has worked well for surfaces with unit cells that are not too large (e.g. up to a (7x7) unit cell when using all available symmetries[17,18]), but is generally not suitable for nanostructures due to their hundreds or thousands of inequivalent atoms.

2.1 Iterative methods vs. inversion. Scaling

Let us suppose that the dimension of the $Ax = b$ problem is N. Then the matrix A contains N^2 elements which must be stored in memory. Determining the inverse of this matrix scales as N^3. In the standard LEED case, if there are n atoms in the unit cell and the electron wavefunction's maximum order of expansion in spherical waves is $l_{\max}$, then the problem's dimension is $N = (l_{\max} + 1)^2 \times n$. Thus, the computation complexity scales with the cube of the number n of inequivalent atoms and the memory requirement for the A matrix storage is proportional to the square of n. When the system of interest is a surface with up to tens of atoms per unit cell, the inversion method requires reasonably small resources both in terms of computation time and memory.

However, when one studies nanostructures, the long-range periodicity assumed by most LEED codes may not be present at all, or if it exists, the number of atoms in the unit cell

may become as high as several hundreds or more. For LEED calculations performed on nano-systems ("nanoLEED calculations"), we will thus need to assume that no long-range periodicity is present, so that a cluster approach would be used, rather than the slab approach characteristic of most standard LEED theories. Consequently, the dimension of the $Ax = b$ problem becomes extremely large and the amount of required resources, in terms of both memory and compute power, become prohibitive.

In order to overcome the high calculation complexity, we will solve the matrix-vector equation not by inversion, but by an iterative method that exhibits better than n^2 scaling.

The operations with highest numerical complexity of any step of an iterative algorithm that solves the $Ax = b$ equation are the matrix-vector products, so the compute time per iteration step scales as N^2. If N_s steps are required to reach convergence, the total compute time scaling is $N_s \times N^2$. As long as $N_s << N$, the use of an iterative method is a major improvement.

Due to the high complexity of a nanoLEED calculation, lowering the computing effort scaling to N^2 and not lowering the memory requirement is not sufficient. Therefore, we have implemented more efficient methods which lower both the computational effort and the memory requirement of LEED calculations for nanostructures. In order to achieve this goal, our methods operate with an approximate matrix instead of the full A matrix.

2.2 The (Bi)Conjugate gradient method

Not all the iterative methods can accept the lowering of their computational and memory requirements without significant loss in accuracy (thus being suitable for our aim), nor do all the methods that are suitable for our goal accept the same level of approximation and still produce accurate solutions. Amongst the methods we tested so far, the most suitable iterative method for nanoLEED calculations was found to be the BiConjugate Gradient (BiCG) method[19]. This is an enhancement of the standard Conjugate Gradient (CG) method[20] conceived for a hermitian matrix.

Since in LEED the multiple scattering matrix is usually not hermitian, BiCG has to be used instead of CG. The main difference between CG and BiCG is that the latter also considers the adjoint matrix-vector equation associated to the original $Ax = b$, namely $x^* A^* = b^*$. The CG method generates successive sets consisting of an approximate solution, corresponding residuals and the search directions to be used in the next iteration step. At each iteration, two inner products are performed in order to compute updated scalars that are defined such that certain orthogonality conditions are satisfied. If the A matrix is hermitian, these conditions imply that the distance to the correct solution is minimized in norm. In the case of a non-hermitian matrix, the inclusion in the algorithm of the adjoint equation implies the replacement of the orthogonal sequence of residuals by two mutually orthogonal sequences that are simultaneously minimized at each iteration. If the residual norm satisfies a certain stopping criterion, the approximate solution is close enough to the correct one and the algorithm stops. In practice, our

stopping criterion for the NanoLEED case is chosen such that the residual norm at convergence must be as low as 0.0075% of the initial residual norm in order to guarantee a high accuracy (higher than 99%) in the final intensities. However, for some systems the convergence has been found to become extremely slow. So we chose to stop the algorithm as soon as the improvement in residual norm becomes smaller than 0.0001% per iteration. We find that the precision attained is nonetheless high enough in practice (less than 2% error).

The character of the system matrix A determines whether the BiCG method converges fast or slow, or not at all. To analyze this, we must use the concepts of matrix rank and condition number. In linear algebra, the rank of a matrix is the number of linearly independent rows or columns of that matrix, i.e. the number of non-zero eigenvalues. Each linearly independent row or column is an eigenvector of the matrix and corresponds to an eigenvalue. In practice, since in LEED eigenvalues are non-zero in general, we ignore eigenvalues smaller than some fraction of the largest eigenvalue to define the rank of matrix A.

If we denote by A^* the hermitian conjugate of a matrix A, there is a set of real positive numbers called "singular values" $\{\sigma_i(A)\}_i$ and two sets of non-zero vectors, $\{u_i\}_i$ and $\{v_i\}_i$ (of identical length), such that

$$\begin{cases} Au_i = \sigma_i(A)v_i \\ v_iA^* = \sigma_i(A)u_i \end{cases}$$

The singular values $\{\sigma_i(A)\}_i$ are of special importance for numerical studies. With $\|A\|$ the norm of matrix A, the condition number of that matrix is defined as $\kappa(A) \equiv \|A^{-1}\| * \|A\|$ and, if the spectral norm $\|A\| = \sqrt{\sigma_{\max}(A)}$ is used, the condition number can be expressed simply as

$$\kappa(A) = \frac{\sigma_{\max}(A)}{\sigma_{\min}(A)}$$

where $\sigma_{\max}(A)$ and $\sigma_{\min}(A)$ are the largest and smallest singular values of matrix A, respectively.

The condition number is a measure of how well-posed the numerical problem of solving the matrix-vector equation is (according to Hadamard, a well-posed problem has a unique solution which depends continuously on the parameters of the problem in a reasonable topology). A problem with a high condition number is said to be ill-conditioned, while a low condition number corresponds to a well-conditioned problem. In the case of BiCG, a low condition number will mean a reliable and fast convergence, whereas a high condition number will mean a slow convergence, or none. In LEED, the complete scattering matrix has elements equal to unity on the main diagonal; thus, in order to

achieve a fast BiCG convergence due to good conditioning, the matrix elements should all be smaller than unity and decrease gradually in absolute value away from the main diagonal toward small values in the off-diagonal corners.

At each iteration step one needs to perform two matrix-vector products of type Ax , which need $O(n^2)$ compute times. As we stated earlier, the goal of our fast methods is to find reasonable approximations of matrix A to lower the complexity of the matrix-vector product.

2.3 The grid method

One case of special value to increase computational efficiency is when the matrix A is periodical, *i.e.* satisfies the condition

$$A_{m,n} = A_{m+p,n+p} \equiv a_{m-n}$$

for all m and n and for any integer $p < N$. In this case, we have

$$\begin{pmatrix} A_{1,1} & A_{1,2} & A_{1,3} & \cdots & A_{1,N} \\ A_{2,1} & A_{2,2} & A_{2,3} & \cdots & A_{2,N} \\ A_{3,1} & A_{3,2} & A_{3,3} & \cdots & A_{3,N} \\ \vdots & \vdots & \vdots & \ddots & \vdots \\ A_{N,1} & A_{N,2} & A_{N,3} & \cdots & A_{N,N} \end{pmatrix} = \begin{pmatrix} a_0 & a_{-1} & a_{-2} & \cdots & a_{1-N} \\ a_1 & a_0 & a_{-1} & \cdots & a_{2-N} \\ a_2 & a_1 & a_0 & \cdots & a_{3-N} \\ \vdots & \vdots & \vdots & \ddots & \vdots \\ a_{N-1} & a_{N-2} & a_{N-3} & \cdots & a_0 \end{pmatrix}$$

and a is a vector of length $2N-1$. The matrix A is called a Toeplitz matrix, and contains only $2N-1$ independent elements, instead of N^2. For this class of matrices, the Ax - type matrix-vector product can be performed more efficiently than the usual N^2 scaling. First, one can write explicitly, in this particular case, the matrix-vector multiplication elements as

$$b_n = (Ax)_n = \sum_{m=0}^{N-1} a_{n-m}\, x_m$$

which can be immediately recognized as a linear convolution. We know that for a circular convolution, *i.e.*

$$b_n = (Ax)_n = \sum_{m=0}^{N-1} a_{(N-m) \bmod N}\, x_m$$

the convolution theorem applies, and

$$\mathsf{F}(b) = \mathsf{F}(Ax) = \mathsf{F}(a) * \mathsf{F}(x)$$

where by $\mathsf{F}(x)$ we denote the Discrete Fourier Transform (DFT)[21] of the vector x and "$*$" denotes the multiplication in reciprocal space. The main computational effort lies now not in the multiplication itself, but in the Fourier transform; but this can be done with $O(N\log N)$ efficiency using the Fast Fourier Transform (FFT) algorithm[22] for DFT. Thus, the computational complexity of the original matrix-vector multiplication can be lowered to $O(N\log N)$ if the linear convolution can be rewritten as a circular convolution. This is equivalent to transforming the initial Toeplitz matrix into a circulant matrix (the rows or columns of this type of matrix are circular permutations of the first row or column). As there are $2N-1$ independent elements in the initial matrix, the easiest manipulation is to embed the $N \times N$ Toeplitz matrix A in a $2N \times 2N$ circulant matrix A' with the aid of an auxiliary $N \times N$ matrix A'':

$$A'' = \begin{pmatrix} 0 & a_{N-1} & a_{N-2} & \cdots & a_2 & a_1 \\ a_{1-N} & 0 & a_{N-1} & \cdots & a_3 & a_2 \\ a_{2-N} & a_{1-N} & 0 & \cdots & a_4 & a_3 \\ \vdots & \vdots & \vdots & \ddots & \vdots & \vdots \\ a_{-2} & a_{-3} & a_{-4} & \cdots & 0 & a_{N-1} \\ a_{-1} & a_{-2} & a_{-3} & \cdots & a_{1-N} & 0 \end{pmatrix}$$

The initial vector x of length N is extended to a vector x' of length $2N$, with

$$x'_n = \begin{cases} x_n, n \le N, \\ 0, n > N. \end{cases}$$

A new $2N$ - dimensional matrix-vector multiplication is constructed:

$$A'x' = \begin{pmatrix} A & A'' \\ A'' & A \end{pmatrix} \begin{pmatrix} x \\ 0 \end{pmatrix} = \begin{pmatrix} b \\ 0 \end{pmatrix}$$

The first N elements of the new matrix-vector product form the vector b, the result of the desired matrix-vector multiplication. Using FFT, this can be calculated with $O(N\log N)$ efficiency. However, the use of FFT imposes a constraint on N, which must be an integer power of 2.

From the point of view of LEED, the physical situation corresponding to the mathematical case described here has atoms situated on a perfect 1D, 2D or 3D rectangular grid (the 2D and 3D cases are simple extensions to more dimensions of the algorithm presented above), containing $N_g = 2^k$ gridpoints (k integer). In nature, particularly in nanostructures, it is highly unlikely that atoms would be perfectly arrayed on such a grid. We can nonetheless use this type of grid algorithm to treat a real physical situation with atoms placed in non-grid positions, as described in Section 3.2.

2.4 The UV method

Using the Singular Value Decomposition (SVD) method, any $N \times N$ matrix A can be decomposed into a product of a $N \times r$ matrix U and a $r \times N$ matrix V, where r is the rank of matrix A. The original $A_{N\times N} x_N$ product can then be written as $U_{N\times r} V_{r\times N} x_N$. This lowers the computational complexity from N^2 to $2rN$ and if r is significantly lower than $N/2$ there is a gain in compute speed. However, the SVD algorithm needed to determine the U and V matrices has to process the N rows and columns of the matrix A, leading to $O(N^3)$ computational complexity, which shifts the weight of the calculation on finding the U and V matrices and makes the method seemingly unappealing.

The UV method[23] is an approximation exploiting prior knowledge of or prediction for the value of the rank r. If one can predict or estimate a certain value r_e for the rank of the matrix A, then the decomposition can be performed considering not the entire matrix A, but only r_e linearly independent rows and columns *sampled* from the matrix A. This way, the decomposition complexity is lowered to $N r_e^2$ and so its computational weight is drastically reduced, since the bulk of the calculation is spent on the matrix-vector multiplication.

By "sampling" we mean an algorithm that can select from the rows and columns of the matrix A a set of r_e linearly independent rows and r_e linearly independent columns. To ensure the accuracy of the method, one must overestimate the rank r of A when predicting the value of r_e ($r_e \geq r$) and, in order to ensure a high method efficiency, the difference between estimated and real rank should be as low as possible ($r_e \cong r$). This is achieved in practice by using empirical values obtained from prior studies on the system of interest.

3. Application to "NanoLEED"

3.1 Mathematical formulation of LEED

The standard LEED theory assumes that the atoms are arrayed in a semi-infinite stack of infinite periodical layers. For each layer, transmission and reflection matrices are calculated and total reflected beam intensities are obtained for the stack. This approach takes advantage of the long-range periodicity of bulk structures and surfaces. The LEED pattern of such an ordered structure shows sharp spots mimicking the reciprocal lattice.

In the case of nanostructures, long-range order may not exist; the above described approach will then not work and the LEED pattern will have diffuse intensities rather than sharp spots.

Our method considers the general case in which the electron beam impinges on a certain region of a nanomaterial or a region of a surface covered with one or more nanostructures. A cluster of all the atoms contributing to electron scattering is formed and exit-direction-dependent intensities reflected by the whole cluster of atoms are calculated for certain directions chosen to match the experimental intensities. The incident electron beam may be collimated (a plane wave) or convergent: we wil lonely discuss the collimated case here, and defer the convergent case to a separate publication[7].

In order to determine the reflected beam intensities, we first obtain the scattering matrices T_i representing the effect of all the scattering paths which an electron may follow inside the cluster and which end at atom i. These quantities are the solution of the matrix-vector equation

$$\mathbf{t} = (\mathbf{I} - \mathbf{tG})\mathbf{T} \tag{1}$$

where, if we denote by $L \equiv (l, m)$ the pair of angular momentum quantum numbers:

$\mathbf{t}$ is a block-diagonal matrix composed of atomic scattering matrices $\mathbf{t}^i$ for individual atoms, $\mathbf{t}^i = (t^i_{LL'})$, $t^i_{LL'} = t^i_l \delta_{ll'} \delta_{mm'} \propto e^{i\delta_l} \sin\delta_l \, \delta_{ll'} \delta_{mm'}$

$$\mathbf{T} = (T_{LL'})$$

$$\mathbf{I} - \mathbf{tG} = \begin{pmatrix} \mathbf{I} & -\mathbf{t}^1\mathbf{G}^{12} & -\mathbf{t}^1\mathbf{G}^{13} & \cdots & -\mathbf{t}^1\mathbf{G}^{1n} \\ -\mathbf{t}^2\mathbf{G}^{21} & \mathbf{I} & -\mathbf{t}^2\mathbf{G}^{23} & \cdots & -\mathbf{t}^2\mathbf{G}^{2n} \\ -\mathbf{t}^3\mathbf{G}^{31} & -\mathbf{t}^3\mathbf{G}^{32} & \mathbf{I} & \cdots & -\mathbf{t}^3\mathbf{G}^{3n} \\ \vdots & \vdots & \vdots & \ddots & \vdots \\ -\mathbf{t}^n\mathbf{G}^{n1} & -\mathbf{t}^n\mathbf{G}^{n2} & -\mathbf{t}^n\mathbf{G}^{n3} & \cdots & \mathbf{I} \end{pmatrix} \equiv \mathbf{C} \tag{2}$$

is the complete scattering matrix of the cluster, and

$$\mathbf{G}^{ij} = (G^{ij}_{LL'}) \text{ and } G^{ij}_{LL'} = -8\pi i k_0 \sum_{L''} i^{l''} h^1_{l''}(k_0 r_{ij}) Y_{L''}(\hat{r}_{ij}) a(L, L', L'')$$

is the free electron Green function between atoms i and j, where

$a(L_1, L_2, L_3) = \int Y^*_{L_1}(\Omega) Y_{L_2}(\Omega) Y^*_{L_3}(\Omega) d\Omega$ is a Clebsch-Gordon coefficient

$h^1_l(z)$ is a Hankel function of the first kind and

k_0 is the incident electron's wave number.

The core of the calculation lies in solving the matrix-vector equation (1). As discussed earlier, the method chosen is not the matrix inversion, but the iterative BiCG; however, the N^2 scaling of BiCG is not satisfactory, so we select more efficient methods presented in Sections 2.3 and 2.4

3.2 The Sparse Matrix Canonical Grid (SMCG) method

Let us suppose for a moment that the nanosystem of interest is a linear chain of N_g chemically identical atoms, equally spaced. Then, for a given pair of angular momentum indices L and L',

$$G_{L\,L'}^{n\,m} = G_{L\,L'}^{n+p,\,m+p} = g_{L\,L'\,n-m}$$

for any atoms n and m in the chain and for any p such that $n + p \le N$ and $m + p \le N$. Consequently, the matrix $\mathbf{C}$ (eq. 2) of the linear chain has the same property, *i.e.*

$$C_{L\,L'}^{n\,m} = C_{L\,L'}^{n+p,\,m+p}$$

At each step of the BiCG iteration, two matrix-vector products have to be performed, both involving either the scattering matrix and a chain-related vector, $\mathbf{p} = (p_L^n)$, or their adjoint counterparts. As the adjoint product is numerically similar to the direct product, we will only present the latter; all the mathematical manipulations valid in the direct case will work with minimal modifications for the adjoint counterpart.

One can see that by reordering the operations as

$$q_L^n = \sum_{L',m} C_{L\,L'}^{n\,m} p_{L'}^m = \sum_{L'} \left[\sum_m C_{L\,L'}^{n\,m} p_{L'}^m \right]$$

the sum inside the square brackets is a linear convolution, which can be performed with $O(N_g \log N_g)$ efficiency by FFT (see section 2.3) if the number of atoms in the chain is an integer power of 2.

Generally, the systems of interest in nanoscience are three-dimensional; let us first suppose that the system studied forms a rectangular 3D grid of N_g chemically equivalent atoms, while on each of the three basis directions of the grid there are N_{g1}, N_{g2} and N_{g3} atoms, respectively. Each atom can be labeled by its three grid indices n_1, n_2 and n_3 so the direct matrix-vector products to be performed at each iteration step can be written as

$$q_L^{n_1,n_2,n_3} = \sum_{L',m_1,m_2,m_3} C_{L\,L'}^{n_1,n_2,n_3,\;m_1,m_2,m_3} p_{L'}^{m_1,m_2,m_3} = \sum_{L'} \left[\sum_{m_1,m_2,m_3} C_{L\,L'}^{n_1,n_2,n_3,\;m_1,m_2,m_3} p_{L'}^{m_1,m_2,m_3} \right]$$

As for the 1D case (linear chain) the sum inside the square brackets is a linear convolution, three-dimensional this time, and can be performed by 3D-FFT with $O(N_g \log N_g)$ efficiency, with $N_g = N_{g_1} N_{g_2} N_{g_3}$.

However, it is in reality unlikely that the atoms are all identical and arranged on a rectangular 3D grid. We can nonetheless take full advantage of this $O(N_g \log N_g)$ efficient method for any given system of interest. Let us suppose that the nanostructure under study is a random cluster of atoms with random chemical species. If one arranges within this cluster a rectangular 3D grid, each atom can be "assigned" to its closest grid point. The propagation of the electron wavefunction between atoms i and j can be seen as three successive processes (figure 1): first, the electron wave originating from point i is re-expanded with respect to grid point A; then, the resulting wave is propagated to the grid point B; and finally, the electron wave resulting at grid point B is re-expanded around the point j. In other words, the Green function calculated between two atoms i and j can be expressed in terms of the Green function related to the corresponding closest grid points A and B:

$$-t_l^i G_{LL'}^{ij} = \sum_{L_A} \sum_{L_B} \tilde{J}_{LL_A}^{iA} G_{L_A L_B}^{AB} J_{L_B L'}^{Bj} \tag{3}$$

where $\tilde{J}_{LL_A}^{iA}$ and $J_{L_B L'}^{Bj}$ are the so-called "shift matrices" and their mathematical expressions are

$$\tilde{J}_{L_i L_A}^{iA} = -4\pi t_i^l \sum_L i^l j_l(k_0 r_{iA}) Y_L(\hat{r}_{iA}) a(L_i, L_A, L)$$

$$J_{L_B L_j}^{Bj} = 4\pi \sum_L i^l j_l(k_0 r_{Bj}) Y_L(\hat{r}_{jB}) a(L_i, L_j, L)$$

with $j_l(z)$ a spherical Bessel function of the first kind.

Now the total cluster scattering matrix $\mathbf{C}^{ij}$ can be expressed in terms of the grid counterpart $\mathbf{C}^{AB}$ by a relation similar to (3) and the direct matrix-vector product of a BiCG step can be written as

$$q_L^i = \sum_{L_A} \tilde{J}_{LL_A}^{iA} \sum_{L_B} \left[\sum_B C_{L_A L_B}^{AB} \left(\sum_{L'} J_{L_B L'}^{Bj} p_{L'}^j \right) \right] = \sum_{L_A} \tilde{J}_{LL_A}^{iA} \sum_{L_B} \left[\sum_B C_{L_A L_B}^{AB} \tilde{p}_{L_B}^B \right] \tag{4}$$

After the sum inside the parentheses is performed, the sum inside the square brackets is a linear 3D convolution; if the grid's dimensions are integer powers of 2, it can be performed by 3D-FFT with $O(N_g \log N_g)$ efficiency. By N_g we understand the total number of grid points on the 3D rectangular grid.

To summarize, the matrix-vector product is performed in three steps: firstly, the atom-to-atom path is made to pass through the grid points nearest to the two atoms; secondly, the grid-related matrix-vector product is performed with $O(N_g \log N_g)$ efficiency; and finally, the grid-related result is shifted back to the corresponding atomic positions. As the shift operations are of a complexity proportional to the square of the cutoff in angular momentum $l_{\max}$ (typically around 7), the bulk of the calculation is the grid-related product, performed efficiently by FFT. This is the Sparse Matrix Canonical Grid (SMCG) method originally developed for electromagnetic waves[20].

The accuracy of the decomposition (4) depends upon the cutoff $l_{\max}$ in the sums over L_A and L_B. The larger the shift from an atom i to the nearest grid point A, the larger the cutoff should be in order to maintain accuracy, which may dramatically increase the computational burden. The cutoff can be reduced by using a denser grid, thus shortening the required shifts, but this may result in many more grid points than atoms, again increasing the burden.

For reasonable cutoff and maximum shift, the decomposition (3) does not ensure accuracy if the atoms are closer than a certain critical distance, which may be several atomic diameters. A solution is then to split the scattering matrix into a sum of two matrices, one containing the electron propagations between atoms closer than this critical distance and the other containing propagations between more distant atoms. The matrix-vector product accordingly splits into two terms: one that can be obtained with $O(N_g \log N_g)$ efficiency, using FFT, and one that must be calculated by the classical method. Fortunately, the class of distant atoms is normally much more populated than the other for typical nanostructures (*e.g.* carbon nanotubes), so the major part of the calculation is performed with high efficiency.

3.3 The "UV" method for LEED

As stated in section 2.4, both the efficiency and the accuracy of the "UV" method depend on the sampling of rows and columns fed into the algorithm. It is vital that the sampling include the largest possible set of linearly independent rows and columns of the matrix. For the case of electromagnetic wave scattering several schemes exist for sampling linearly independent rows and columns out of the complete scattering matrix[23], but for the electron scattering case the development of effective sampling algorithms is not yet complete. So far, our sampling schemes can handle a system of just two scatterers. In the case of electromagnetic waves, the UV decomposition yields a matrix-vector product efficiency of $O(n \log n)$, n being the number of scattering particles[23]. For LEED, if the UV method can only be applied to small matrices corresponding to pairs of scatterers, this order of efficiency cannot be achieved. However, since the sub-matrix dimension is $(l_{\max}+1)^2$, which is 64 for $l_{\max} = 7$, and the rank has a maximum estimated value of 15

and decreases rapidly with the distance between the two scatterers (figure 2), the use of UV decomposition still typically speeds up the computation by a factor larger than 6 compared to standard matrix-vector inversion.

3.4 Application to LEED: SMCG vs. UV vs. direct calculation

To test our methods, we performed LEED calculations on buckminsterfullerenes (C_{60}). It is known experimentally that these molecules can order as adsorbates with (4x4) periodicity on a Cu(111) single-crystal substrate: we chose this geometry to test the numerical accuracy of our NanoLEED calculations, while removing the Cu atoms from the computation (the substrate will be included in our modeling in section 5). We continued to identify the beam directions using the Cu(111) reciprocal lattice, resulting in quarter-order beam labels. To that end, we calculated standard "I-V curves" (intensities as a function of voltage or energy). We chose a realistic $l_{\max} = 7$ and an inelastic potential of $V_i = -5eV$.

As after a cutoff distance d_{cut} the electron wave will be largely attenuated by the crystal due to damping, the atoms composing the cluster used in calculation were those of the (4x4) unit cell and all their periodically equivalent atoms that are translated by at most d_{cut}.

In figure 3 we compare I-V curves for selected LEED beams calculated by different methods for a periodic monolayer of pure C_{60} (the cluster used in the calculations contained 376 atoms). A well-converged CG result represents the "correct" solution (correct within the usual physical model of LEED theory). It serves as reference for approximate SMCG and UV results, as well as for a combined CG+SMCG+UV approach described below. The SMCG calculation used a three-dimensional grid spacing of 0.4 nm. The UV calculations typically yielded ranks ~17% of N. All four methods needed exactly the same number of iterations to reach convergence.

The calculations performed with different methods are seen to yield visually indistinguishable curves, thus verifying the accuracy of the SMCG and UV methods, and their combination.

As a measure of relative computing speed, at 100 eV, our computer yielded compute times per iteration for these CG, SMCG and UV results of 252.81, 77.75 and 94.65 seconds, respectively.

Let us now discuss in more detail the relative performances of CG, SMCG and UV observed in our LEED tests. We find that each method outperforms the others in specific circumstances, so that a combined approach will be most appropriate overall.

First, SMCG is most effective in LEED when dealing with a large number of atoms. This

is due to the fact that the time-consuming, grid-related results are common to all atoms closest to the same grid point. Secondly, SMCG tolerates a relatively low $l_{\max}$ to properly describe pairs of distant atoms but needs higher $l_{\max}$ for closely-packed atoms. Thus, SMCG outperforms CG and UV for large numbers of atoms and large interatomic distances.

The accuracy of the UV method depends on the abovementioned sampling of rows and columns and does not depend on the value of $l_{\max}$. However, for pairs of very close atoms (spaced less than 0.2 nm) the rank of the pair scattering matrix is very close to the matrix dimension, and the method becomes inefficient. For this reason, direct CG calculations are the most effective for very close neighbors.

We can exploit the relative strengths of CG, SMCG and UV by splitting the initial scattering matrix $\mathbf{C}$ (eq. 2) into three parts, $\mathbf{C} = \mathbf{C}_{CG} + \mathbf{C}_{UV} + \mathbf{C}_{SMCG}$, each of which is then treated with a different method. Here, $\mathbf{C}_{CG}$ includes only atoms closer than 0.2 nm one from another (and the unit matrix $\mathbf{I}$ of $\mathbf{C} = \mathbf{I} - \mathbf{tG}$), which are best treated by CG; $\mathbf{C}_{UV}$ includes atoms with intermediate separations, best treated by UV; and $\mathbf{C}_{SMCG}$ includes only distant atom pairs and is treated by SMCG. This decomposition has been used for rough-surface scattering problems under the name "UV-SMCG"[21].

Consequently, the compute time per iteration has three additive components, with compute times that scale differently: for SMCG it scales as $N_g \log N_g$, where the number of grid points N_g is normally smaller than the number of atoms in the cluster; for the CG method the compute time scales as the cube of the (relatively small) number of closest pairs of atoms; and for UV as $N_{UV}\, r_e^2$, where N_{UV} is the (also relatively small) number of UV-treated pairs of atoms, and $r_e < N$ is the estimated rank of the matrix A. Thus the overall performance of the combined CG+SMCG+UV approach depends on the structure type, since the three methods will occupy different fractions of the computation.

We found that, for large nanostructures, the SMCG part strongly dominates the measured compute times, so the overall time approaches its favorable $N_g \log N_g$ scaling. As an example, if a Cu(111) substrate is added to the C_{60} layer, the number of atoms included in the LEED calculations roughly doubles (848 atoms). Then, each iteration step at 100eV is completed in 68.83 seconds: 9.20 seconds for the UV part; 2.51 seconds for the CG part; and 57.12 seconds for the SMCG part. Figure 4 verifies that the combined method approaches the $N_g \log N_g$ scaling.

It is useful to realize that the SMCG part of the calculation, although by far the most time consuming, contributes typically only ~20% percent of the final intensity. Consequently, if we neglect that part at first and then feed the approximate result into a full-matrix calculation as an initial guess, we can save more than half of the original compute time.

4. Using “NanoLEED”

A central application of LEED has been the atomic-scale structural determination of single-crystal surfaces, thanks to the high sensitivity of I-V curves to changes in atomic positions. We can now prove that the same sensitivity is maintained for nanostructures. Our LEED code “NanoLEED” has been designed to accept a wide variety of types of nanostructure: they include structures with 2D periodicity (e.g. ordered surfaces), with 1D periodicity (e.g. nanotubes or nanowires), and with no periodicity (0D, e.g. isolated or disordered nanoparticles).

In standard LEED, a diffraction pattern with sharp beams results from the periodic surface structure and the collimation and monochromaticity of the incident beam. Most frequently, beam intensities are recorded as a function of electron energy (controlled by an accelerating potential V), yielding “I-V curves”; sometimes, intensities are measured at fixed energy as a function of sample orientation, yielding “rocking curves”. With nanostructures, the two-dimensional periodicity may be lost, resulting in “diffuse” diffraction patterns. This allows other modes of measurement, for example as a function of electron exit direction for fixed sample orientation at fixed electron energy, as has already been exploited in “diffuse LEED” from disordered surfaces[26,27,28]. These various modes of measurement, as well as combinations thereof, can be used to determine nanostructures with LEED, since the resulting data are structure-sensitive. The most appropriate choice of experimental variable will depend on the kind of nanostructure to be solved. In any case, there will be a minimum requirement for a sufficient number of measured data points to permit the determination of the unknown structural parameters, which may be quite numerous (for guidance, a rule of thumb used in LEED for crystalline surfaces is a minimum of 10 peaks in I-V curves for each unknown structural parameter).

5. “NanoLEED” applied to nanostructures

We have chosen to illustrate the application of “NanoLEED” to several types of nanostructure of actual interest. We focus our attention on the structural sensitivity of calculated intensities, to exhibit the potential of the method for structural determination. In the following, the behavior of LEED intensities will be shown for buckminsterfullerenes (buckyballs, C_{60}) and carbon nanotubes (CNTs). The application to non-periodic silicon nanowires will be shown elsewhere[7]. In these calculations, graphite phase shifts were used for C and bulk phase shifts for Cu and Li; the Debye temperatures were 973 K for C, 335 K for Cu and 600 K for Li. The theoretical curves were produced for incident electrons with energies between 50 and 165 eV and for a sample temperature of 300 K. The surface potential step was set to 10 eV and the imaginary part of the potential to -5 eV

5.1 Ordered monolayer of buckminsterfullerenes (C_{60})

We performed NanoLEED calculations for a monolayer of C_{60} molecules, as well as of endohedral and exohedral C_{60} by addition of single Cu or Li atoms within and outside each C_{60}, respectively. For similarity with known structures reported in the literature[29], we ordered these nanostructures as adsorbates with (4x4) periodicity on a Cu(111) single-crystal substrate. Because of the thickness of the C_{60} monolayer, the LEED electrons will not penetrate the substrate much, so we limited the Cu(111) to 4 metal layers, the number of atoms being $n = 124$ or 125 per (4x4) unit cell, without or with a Li or Cu atom, respectively.. Each C_{60} molecule was oriented such that two of its hexagonal rings were located at the top and at the bottom of the molecule, parallel with the Cu(111) layers, the hexagon centers being located over hcp hollow sites (see figure 5); the distance from the bottom of the adsorbate layer to the substrate was 0.2 nm (between planes of nuclei).

For a monolayer of pure C_{60} molecules sitting on the Cu(111) substrate, calculations were performed for three values of the C_{60} radius. In addition to the generally-accepted 0.355 nm radius, we considered a larger radius of 0.375 nm as well as a smaller radius of 0.335 nm. This represents close to a 5% expansion or contraction of the buckyball, respectively, so that individual C-C distances change by about 0.0075 nm (0.075 Å). The spacing between the Cu and the nearest C atoms is kept constant.

As one can see in figure 6, these rather small changes in the molecule radius trigger significant changes in the shapes of the LEED I-V curves; in particular, large shifts of the positions of maxima and minima are observed, which is the usual sign of high structural sensitivity in LEED.

We next considered the possibility of the presence of additional metal atoms inside or outside the C_{60} molecules, as in endohedral or exohedral C_{60}, respectively. Important questions include the position of the additional metal atoms and displacement or distortion of the C_{60} by the additional metal. One additional metal atom per C_{60} molecule represents only one scatterer out of 60+1 scatterers, so that we cannot expect, and did not obtain, high sensitivity to this metal atom by itself. But such an atom will influence its neighborhood, distorting and/or displacing the C_{60}, for instance: this affects many more atoms and should be much more noticeable in LEED.

We added Li or Cu atoms in either of three positions, one per C_{60} molecule (i.e. one per 4x4 unit cell), using realistic interatomic distances: "in and up" positions inside the molecule, 0.143 nm (Li) or 0.174 nm (Cu) above the center of C_{60}, respectively; "in and down" positions inside and 0.143 nm (Li) or 0.174 nm (Cu) below the center of C_{60}, respectively; or "out" position interstitially between C_{60} molecules 0.283 nm (Li) and 0.287 nm (Cu) above the Cu surface. (To simplify the description, we here assume the surface to be “horizontal” with vacuum above it.) If the added metal atom lies inside the sphere, it should modify the electronic structure of its neighbors and consequently their geometrical positions. To simulate this and illustrate the sensitivity of LEED to such effects, we assumed very simple distortions of the buckyballs. Our coarse model supposed that only the C atoms situated in the same spherical cap as the metal atom are affected and the effect is such that the C_{60} sphere is flattened in the area of the respective cap by reducing the vertical C-metal interatomic spacings by 20%; this corresponds to

displacements perpendicular to the surface ranging from 0.003 to 0.03 nm. The I-V curves (figure 7) confirm the expected sensitivity to the supplementary metal atom's presence, or more precisely to its induced distortions; not surprisingly, larger changes in curve shapes are seen for the heavier and thus more strongly scattering atom (Cu vs Li).

5.2 Carbon nanotubes (CNTs)

Another class of test calculations targeted the carbon nanotubes (CNTs). We have chosen for our tests a monolayer of (10,10) armchair single-walled CNTs of 1.36 nm diameter. They are assumed to lie flat on a Cu(111) substrate along the substrate's [112] direction. The matching between the CNT and substrate geometries leads to a (5x7) unit cell on Cu(111), this cell being composed of 200 CNT atoms and 70 substrate atoms in 2 Cu layers.

We have investigated the effect of CNT deformations on the LEED I-V curves. First, we analyzed the possibility of a flattening of the CNTs due to the interaction with the Cu surface. The model assumed that the atoms located below the tube's axis lose a certain percentage of their vertical distance to that axis, keeping the distance between the bottom CNT and the substrate constant at 0.2 nm. First, the tubes are thus flattened by a small 6% vertical compression; then the flattening is increased to 20%. Finally, the upper parts of the tubes are also flattened by 20%, the result being the equivalent of squeezing the nanotubes from both top and bottom. As shown in figure 8, the response to these changes in terms of LEED I-V curves is proportional to the amount of deformation: for a small 6% flattening (corresponding to a maximum 0.082 nm C shift perpendicular to the surface) the effect is small, but for an increased 20% deformation (maximum 0.272 nm shift) the change in shape of the curves is obvious, as it is also in the case of "squeezing" from top and bottom.

Conclusions

We have adapted new, efficient and accurate methods to enable LEED calculations for complex nanostructures, thus permitting their structural determination from LEED experiment. These methods owe their nanostructural capability to the property that they scale basically as $n \log n$, rather than the current n^3 or n^2, with the number of inequivalent atoms n.

Sensitivity of the I-V curves to structural changes was proven and illustrated with LEED calculations performed for different classes of nanosystems. We show here that this feature is present for ordered nanostructures, such as a monolayer of ordered C_{60} adsorbed on Cu(111) or a monolayer of ordered carbon nanotubes adsorbed on Cu(111). The case of isolated or disordered nanostructures will be published separately.

Experimental techniques necessary to perform LEED measurements on ordered nanostructures already exist, while experimental LEED methods have been proposed to focus electron beams in nanoscale areas, and thus on single nanostructures. Given the satisfactory sensitivity and the efficient scaling recorded for LEED simulations, we

believe that detailed structural determination for materials with very large unit cells and for nanoclusters is now possible, a key advance for progress in nanoscience and technology.

Acknowledgments

This work was supported by RGC grant No. CityU1/02C, and in part by the Office of Science, Materials Sciences Division, of the U.S. Department of Energy under Contract No. DE-AC03-76SF00098 while MAVH was at Lawrence Berkeley National Laboratory.

References

[1] Edward L. Wolf, *Nanophysics and Nanotechnology* (Wiley-VCH, Weinheim, 2004).
[2] Guozhong Cao, *Nanostructures and Nanomaterials* (Imperial College Press, London, 2004).
[3] R. Feidenhans'l, Surf. Sci. Rep. **10**, 105 (1989).
[4] See various articles in Principles, Applications, Techniques of EXAFS, SEXAFS, and XANES, edited by D. C. Koningsberger and R. Prins (Wiley, New York, 1988).
[5] R. Wiesendanger, *Scanning Probe Microscopy and Spectroscopy: Methods and Applications* (Cambridge Univ. Press, Cambridge, 1994).
[6] G. M. Gavaza, Z. X. Yu, L. Tsang, C. H. Chan, S. Y. Tong and M. A. Van Hove, Phys. Rev. Lett. **97**, 055505 (2006).
[7] G. M. Gavaza, Z. X. Yu, L. Tsang, C. H. Chan, S. Y. Tong and M. A. Van Hove, in preparation.
[8] T. Sakurai, X.-D. Wang, Q. K. Xue, Y. Hasegawa, T. Hashizume, and H. Shinohara, Prog. Surf. Sci. **51**, 263 (1996).
[9] J. C. Spence, H. C. Poon, and D. K. Saldin, Microscopy and Microanalysis **10**, 128 (2004).
[10] C. S. Fadley, Y. Chen, R. E. Couch, H. Daimon, R. Denecke, J. D. Denlinger, H. Galloway, Z. Hussain, A. P. Kaduwela, Y. J. Kim, P. M. Len, J. Liesegang, J. Menchero, J. Morais, J. Palomares, S. D. Ruebush, E. Rotenberg, M. B. Salmeron, R. Scalettar, W. Schattke, R. Singh, S. Thevuthasan, E. D. Tober, M. A. Van Hove, Z. Wang, and R. X. Ynzunza, Prog. Surf. Sci. **54**, 341 (1997).
[11] S. Mizuno, F. Rahman, and M. Iwanaga, Jpn. J. Appl. Phys., Part 2, **45**, L178 (2006).
[12] S. Amelinckx, et al. (Eds.), Handbook of Microscopy, vols. **487–503**, VCH, Weinheim, 1997.
[13] M. A. Van Hove, and S. Y. Tong, *Surface Crystallography by LEED* (Springer-Verlag, Berlin, 1979).
[14] M. A. Van Hove, W. H. Weinberg, and C. M. Chan, *Low-Energy Electron Diffraction* (Springer-Verlag, Berlin, 1986).
[15] C. H. Chan and L. Tsang, Microwave and Optical Technology Letters **8/2**, 114 (1995).
[16] L. Tsang and Q. Li, Microwave and Optical Technology Letters **41/5**, 354 (2004).
[17] H. Jiang, S. Mizuno and H. Tochihara, Surf. Sci. **380**, L506 (1997).
[18] S.Y. Tong, H. Huang, C.M. Wei, W.E. Packard, F.K. Men, G. Glander and M.B. Webb, J. Vac. Sci. Technol. **A6**, 615 (1988).
[19] R. Barret, M. Berry, T. F. Chan, J. Demmel, J. Donato, J. Dongarra, V. Eijkhout, R. Pozo, C. Romine, and H. Van der Vorst, *Templates for the Solution of Linear Systems: Building Blocks for Iterative Methods*, **2**nd edition (SIAM, Philadelphia, PA, 1994), Vol. **1**, Chap. 2.3.5, p.21.
[20] R. Barret, M. Berry, T. F. Chan, J. Demmel, J. Donato, J. Dongarra, V. Eijkhout, R. Pozo, C. Romine, and H. Van der Vorst , *Templates for the Solution of Linear Systems: Building Blocks for Iterative Methods*, **2**nd edition (SIAM, Philadelphia, PA, 1994), Vol. **1**, Chap. 2.3.1 p.14.
[21] A. V. Oppenheim, R. W. Schafer and J. R. Buck *Discrete-time signal processing*. Upper Saddle River, N.J.: Prentice Hall. 1999.

[22] E. O. Brigham *The Fast Fourier transform and its applications*. Englewood Cliffs, N.J.: Prentice Hall. 1988.
[23] L. Tsang and Q. Li, Microwave and Optical Technology Letters **41/5**, 354 (2004).
[24] C. H. Chan and L. Tsang, Microwave and Optical Technology Letters **8/2**, 114 (1995).
[25] P. Xu and L. Tsang, Radio Science, Vol. 40, RS4012, 2005.
[26] D.K. Saldin, J.B. Pendry, M.A. Van Hove and G.A. Somorjai, Phys. Rev. **B31**, 1216 (1985).
[27] G.S. Blackman, M.-L. Xu, D.F. Ogletree, M.A. Van Hove and G.A. Somorjai, Phys. Rev. Lett. **61**, 2352 (1988).
[28] K. Heinz, U. Starke, M.A. Van Hove and G.A. Somorjai, Surf. Sci. **261**, 57 (1992).
[29] J. E. Rowe, P. Rudolf, L. H. Tjeng, R. A. Malic, G. Meigs, C. T. Chen, J. Chen, and E. W. Plummer, Int. J. Mod. Phys. **B6**, 3909 (1992).

Figure captions:

Figure 1. SMCG method: the electron propagation from atom i to atom j is replaced by a shift from atom i to the nearest grid point A, a propagation to the grid point B closest to atom j and finally a shift from B to j.

Figure 2. For the case of an electron suffering multiple scattering on a system of a pair of scatterers, the scattering matrix rank variation function of the distance between the two scatterers.

Figure 3. Comparison of LEED intensities calculated by different methods described in the text, for a periodic monolayer of C_{60} that mimics a (4x4) layer on Cu(111), absent here, using the corresponding fractional-order beam notation, at normal incidence. Curves are off-set vertically for clarity. (Reproduced from Ref. 6.)

Figure 4. Actual compute times of our combined CG+SMCG+UV approach (points) for different numbers of grid points, representing larger nanoclusters, compared with a $N\log N$ extrapolation of the leftmost point. (Reproduced from Ref. 6.)

Figure 5. Geometry of a C_{60} monolayer sitting on a Cu(111) substrate. Each C_{60} molecule is oriented such that two of its hexagonal rings are located at the top and at the bottom of the molecule, parallel with the Cu(111) layers, the hexagon centers being located over hcp hollow sites. Graphics are generated using © Balsac by K. Hermann, FHI Berlin

Figure 6. Comparison of LEED intensities calculated by NanoLEED for a periodic (4x4) C_{60} monolayer a substrate of 4 layers of Cu(111) for three C_{60} radii. The radius of the C_{60} molecules is varied as indicated, keeping constant the spacing between the Cu and nearest C. (Reproduced from Ref. 6.)

Figure 7. As fig. 6, but adding one atom of Li (at left) or Cu (at right) for each C_{60} molecule, in either of three positions: inside and 0.143 nm (Li) or 0.174 nm (Cu) above the center of C_{60} ("in and up"), or inside and 0.143 nm (Li) or 0.174 nm (Cu) below the center of C_{60} ("in and down"), or interstitially between C_{60}s ("out"), using realistic interatomic distances. In each case, the C_{60} sphere is flattened on the side of the nearest metal atom by reducing the perpendicular C-metal spacings by 20%. (Reproduced from Ref. 6.)

Figure 8. LEED intensities calculated by NanoLEED for a monolayer of (10,10) parallel armchair single-walled CNTs, assumed to lie flat on a Cu(111) substrate along the substrate's [112] direction, inducing a (5x7) unit cell. Undeformed and "squashed" or "squeezed" CNTs are considered, as described in the text.

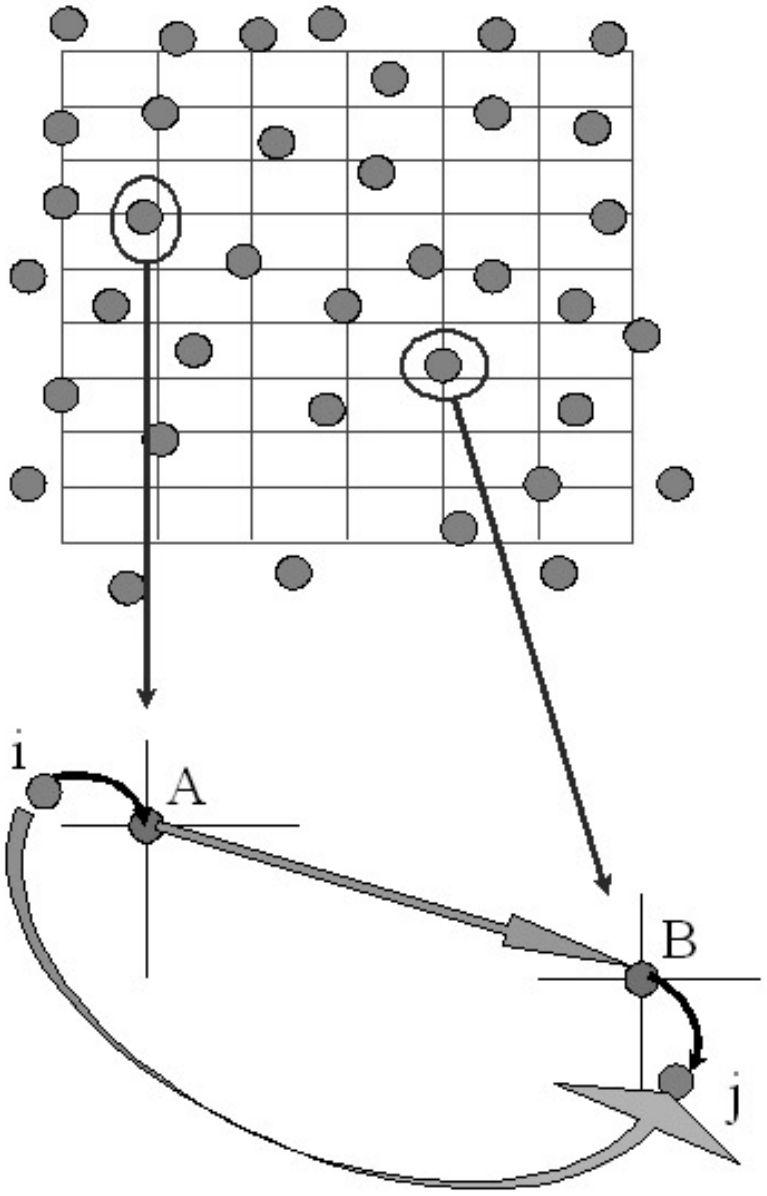

Figure 1

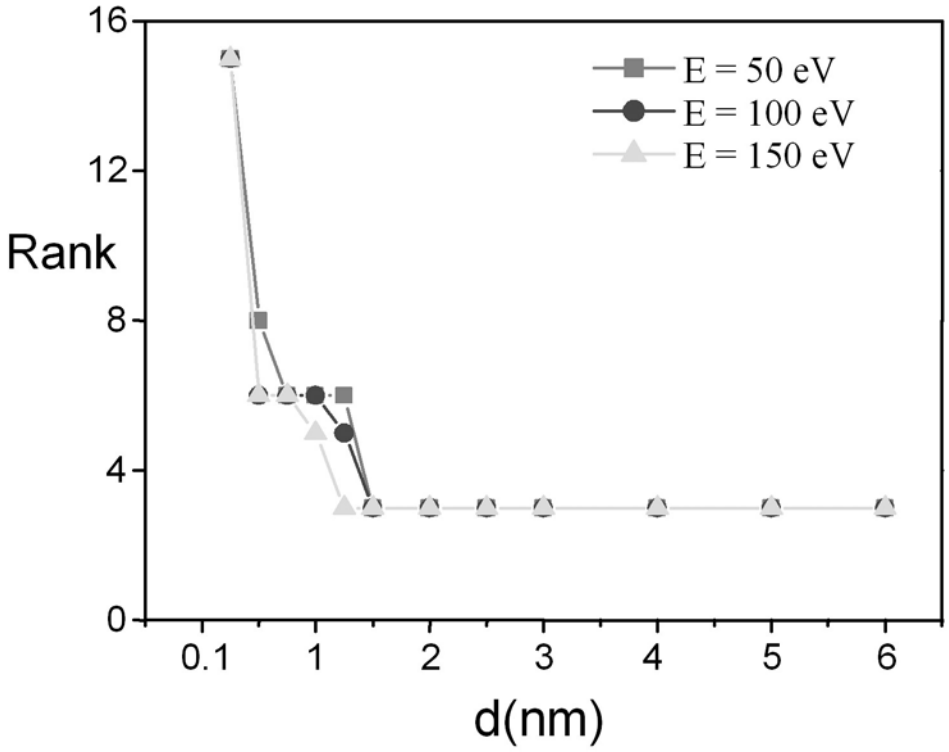

Figure 2

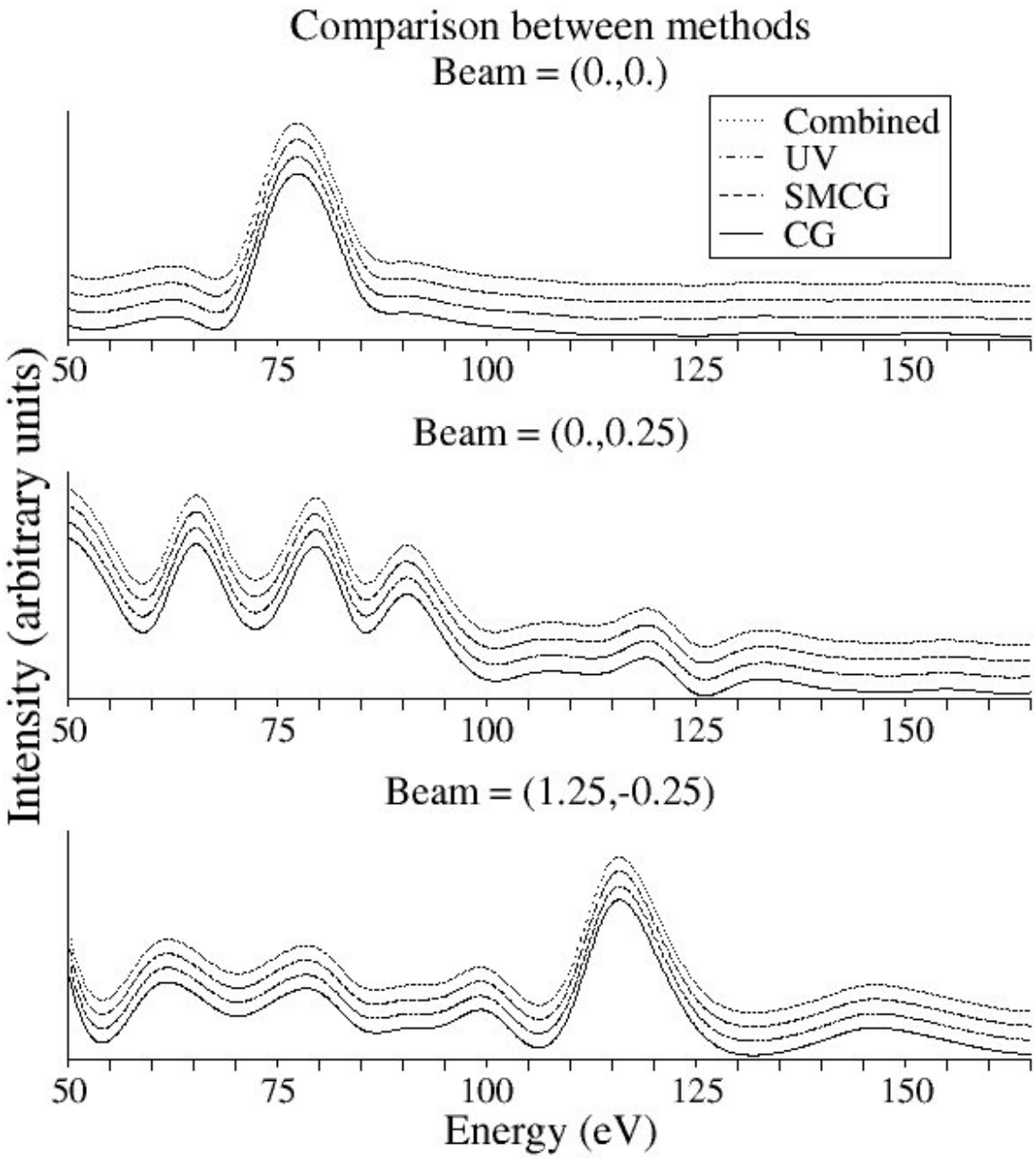
Comparison between methods
Beam = (0.,0.)
Combined
UV
SMCG
CG
Beam = (0.,0.25)
Beam = (1.25,-0.25)
Intensity (arbitrary units)
50
75
100
125
150
Energy (eV)

Figure 3

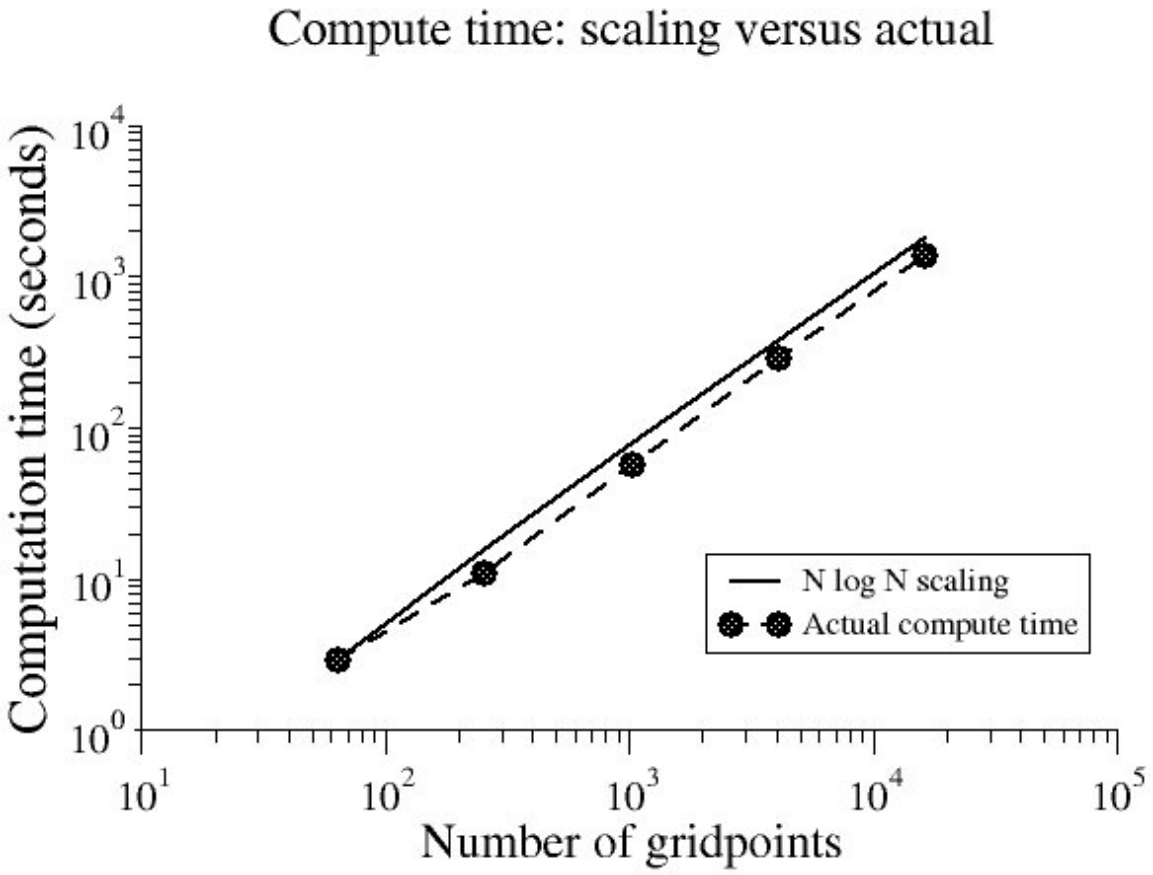
Compute time: scaling versus actual
Computation time (seconds)
10^0
10^1
10^2
10^3
10^4
10^1
10^2
10^3
10^4
10^5
Number of gridpoints
N log N scaling
Actual compute time

Figure 4

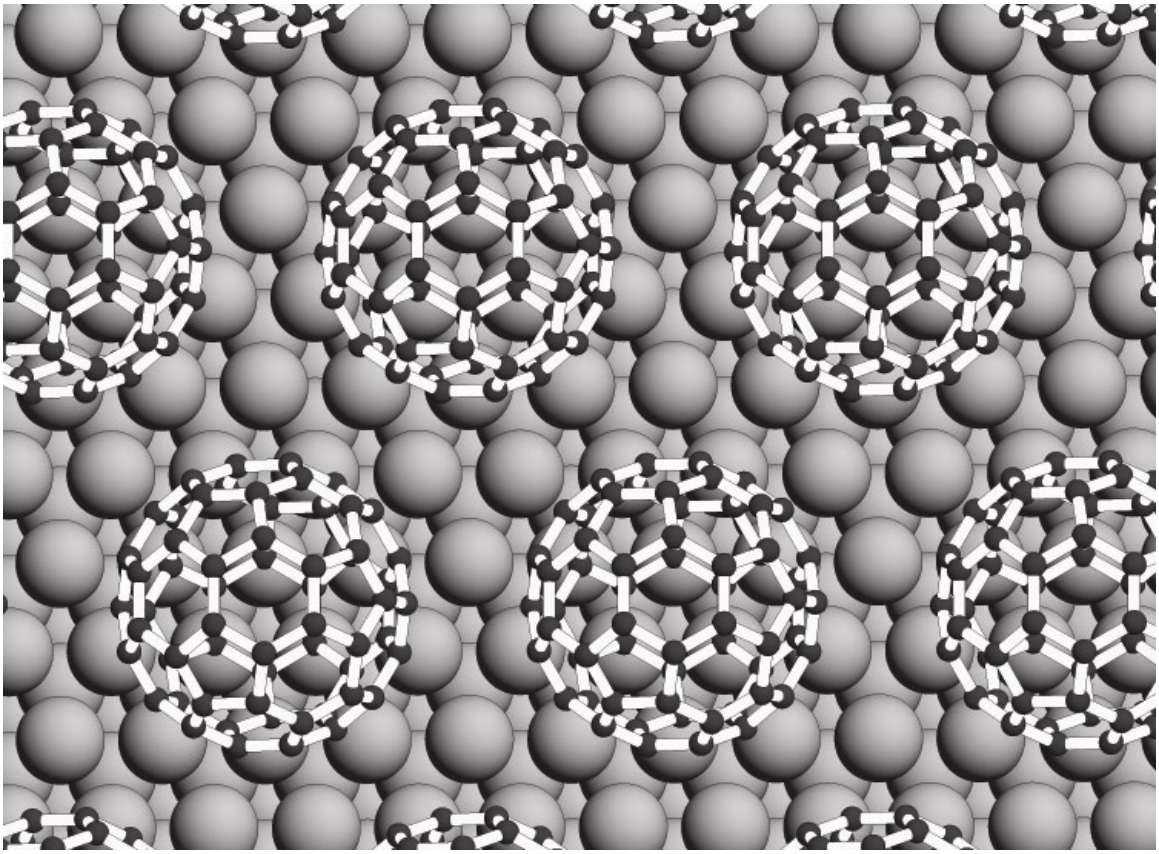

Figure 5

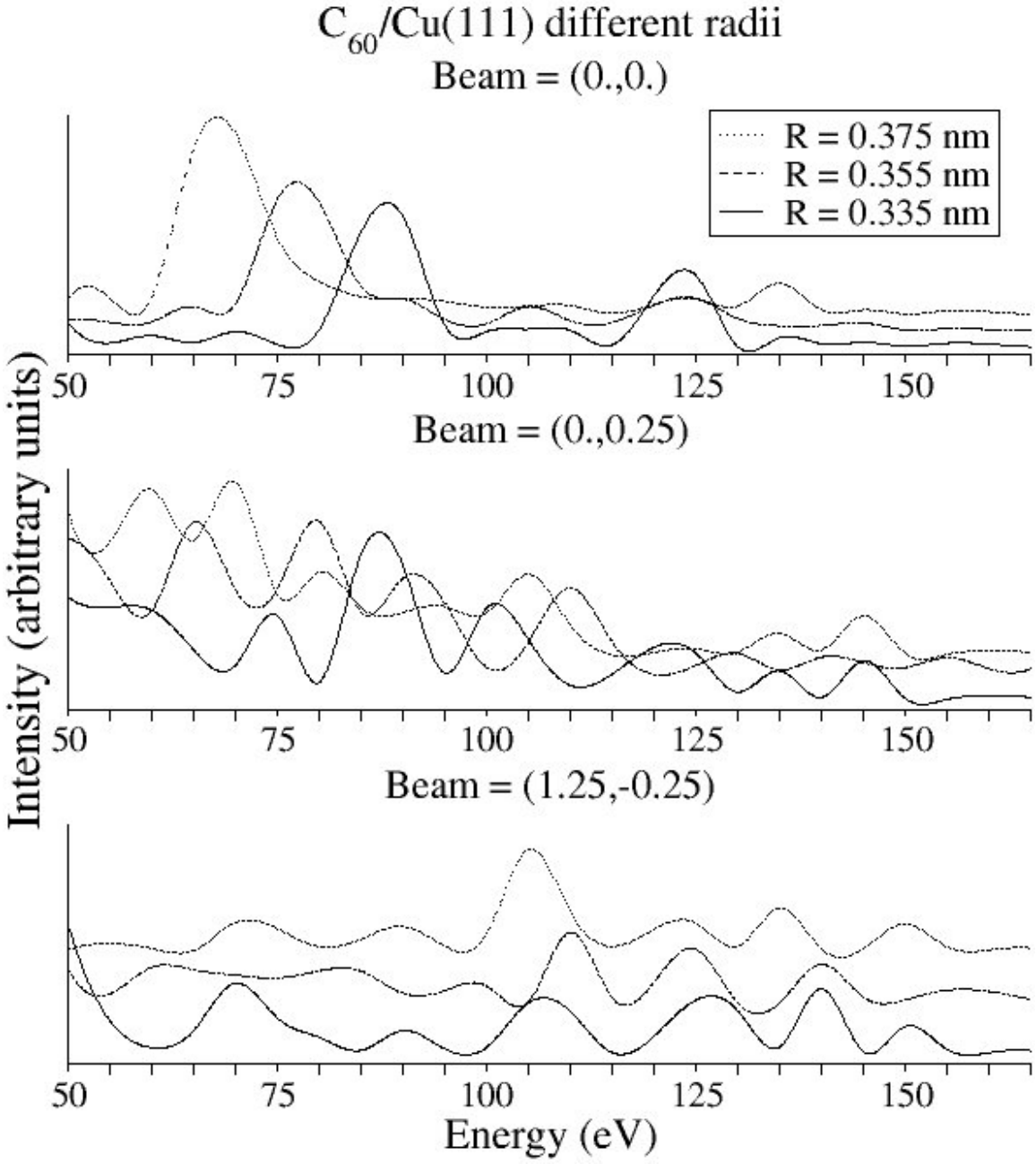
C60/Cu(111) different radii
Beam = (0.,0.)
R = 0.375 nm
R = 0.355 nm
R = 0.335 nm
Beam = (0.,0.25)
Beam = (1.25,-0.25)
Intensity (arbitrary units)
50
75
100
125
150
Energy (eV)

Figure 6

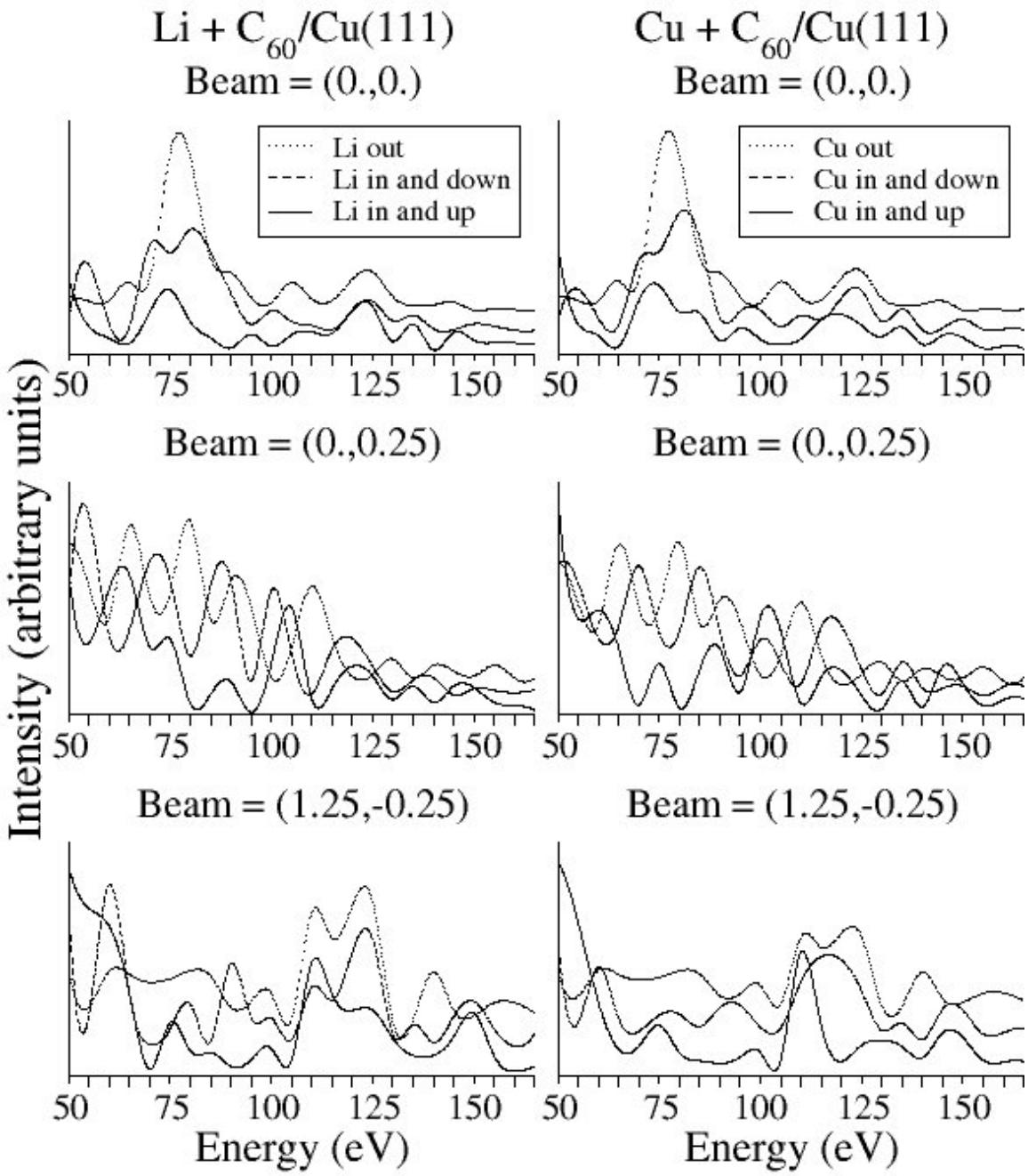
Li + C60/Cu(111)
Beam = (0.,0.)
Li out
Li in and down
Li in and up
Cu + C60/Cu(111)
Beam = (0.,0.)
Cu out
Cu in and down
Cu in and up
Beam = (0.,0.25)
Beam = (0.,0.25)
Beam = (1.25,-0.25)
Beam = (1.25,-0.25)
Intensity (arbitrary units)
50
75
100
125
150
Energy (eV)

Figure 7

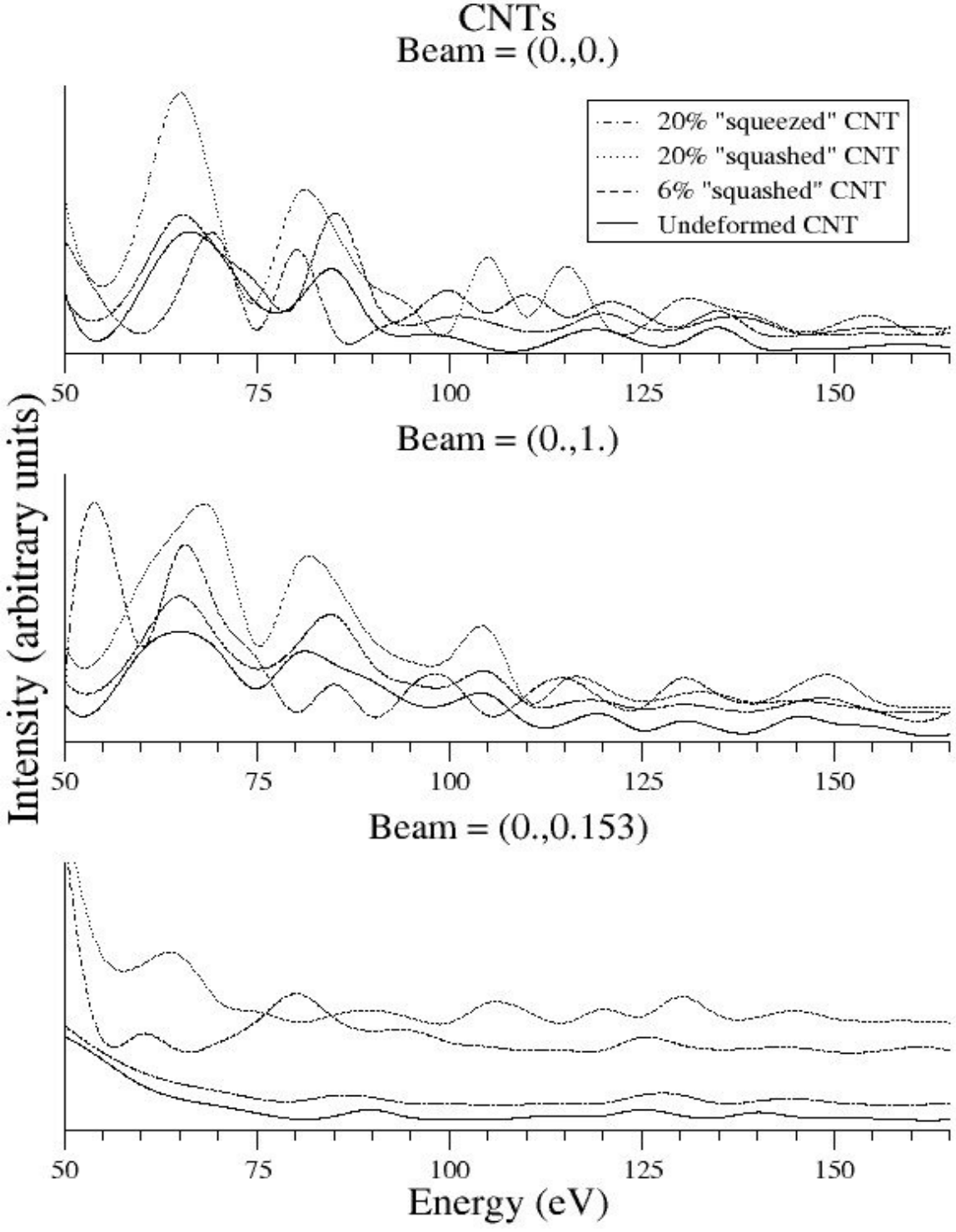
CNTs
Beam = (0.,0.)
20% "squeezed" CNT
20% "squashed" CNT
6% "squashed" CNT
Undeformed CNT
Beam = (0.,1.)
Beam = (0.,0.153)
Intensity (arbitrary units)
50
75
100
125
150
Energy (eV)

Figure 8